Johann Radon Institute for
Computational and Applied Mathematics
Austrian Academy of Sciences (ÖAW)

Modeling the Influence of Unbalances for Ultra-Precision Cutting Processes

J. Niebsch, R. Ramlau, Ch. Brandt, P. Maass

RICAM-Report 2010-09

Modeling the Influence of Unbalances for Ultra-Precision Cutting Processes

Ch. Brandt [1], J. Niebsch[2, *], R. Ramlau [3], and P. Maass [1]

[1] University of Bremen, Bibliothekstrasse 1, 28359 Bremen, Germany
[2] Radon Institute, Austrian Academy of Science,
Altenbergerstr. 69, 4040 Linz, Austria
[3] Johannes Kepler University, Altenbergerstr. 69, 4040 Linz, Austria

Received XXXX, revised XXXX, accepted XXXX
Published online XXXX

Key words ultra-precision cutting machinery, structural rotor model, cutting force model, Inverse Problems, regularization

MSC (2000) 00-xx

In order to produce components in optical quality in ultra-precision cutting processes it is very important to have a highly balanced system. Achieving the best possible balancing state is a time consuming process. Therefore, the prediction of the influence of the balancing state on the surface quality of the component is desirable. On the other hand, such a model should enable us to predict a necessary balancing state for a desired surface quality and thus save time in the balancing process. In this paper we present a model of an ultra-precision cutting experimental platform that determines vibrations and displacements of the platform caused by unbalances and forces from the cutting process. The actual cutting parameters are described by a second model. Since they depend on the unbalance displacements, both models have to be coupled to an interaction model. To compute balancing weights from vibrational measurements, regularization techniques for the solution of inverse and ill-posed problems are employed and presented.

1 Introduction

In order to manufacture components in optical quality like the sample in Figure 1, highly exact cutting machines and diamond tools are necessary. Depending on the form of the intended surface of the workpiece, e.g. plane, spherical or freeform, the workpieces are mounted on-axis or off-axis onto the spindle, and frequently adapters are needed additionally for the mounting. This usually leads to a significant unbalanced system and results in a decreasing quality of the surface. To avoid the latter, high-precision balancing of the spindle including the workpiece is necessary [1]. By balancing, we understand the mounting of additional weights at certain positions at the rotating parts of the machine in such a way that the vibration is reduced below a certain tolerance. A survey of existing balancing methods is given in [2]. At present, the best possible balancing is realized by attaching compensating masses in the balancing plane. Finding the right masses and locations for the balancing weights is a time consuming process. After the cutting process, the construction unit quality is examined. However, to achieve a given surface quality, it might not be necessary to apply a time consuming best possible balancing of the system. Therefore, a prognosis of the attainable workpiece quality based on the unbalance distribution has a substantial economic potential due to a shortened balancing process. To allow for a prediction of the surface quality for a specified balancing state, a model describing the interaction between the engine structure and the machining process is necessary.

Our main aim is the development of such a model for ultra precise cutting machines (UPCM). The model will be used to predict the workpiece quality to be achieved for a given balancing state. On the other hand, the reverse direction will also be covered, i.e., the computation of the necessary balancing state for a given workpiece quality as well as the necessary balancing masses and positions. The investigation of the entire process (balancing state of the rotor-shaft-unit including the workpiece, accuracy of the cutting process, quality of the workpiece) will provide an improvement of the quality of the cutting process of ultra precise tools as well as the determination of quality boundaries for an optimal production process. By providing the necessary balancing weights, the model will significantly shorten the balancing process and thus reduce its time effort and costs.

* Corresponding author E-mail: jenny.niebsch@oeaw.ac.at, Phone: +43 732 2468 5232, Fax: +43 732 2468 5212

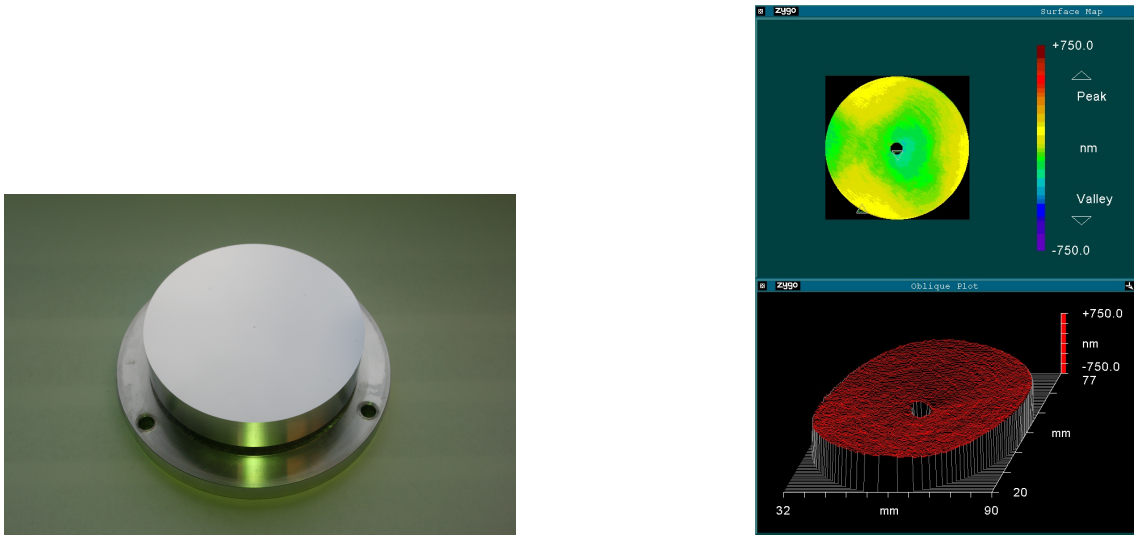

Fig. 1 Sample of a ultra-precision surface workpiece (left) and its surface in detail (right)

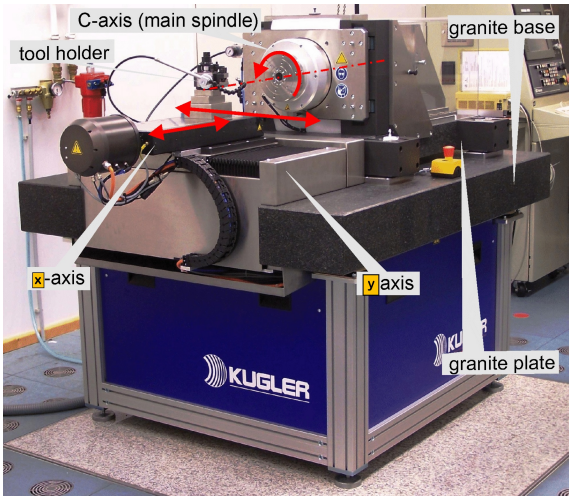

Fig. 2 Experimental platform of an ultra-precise cutting machine at the LFM in Bremen

In a first step, we developed an interaction model for an UPCM experimental platform which is installed at the Laboratory for Precision Machining (LFM) at the University of Bremen, see Figure 2. The platform is designed according to specifications of the LFM and allows for dynamical balancing as well as the modification of parameters like stiffness of the joints. Based on the platform, we have created two sub-models. First, a structure model was developed to determine the vibrations for given force and moment distributions induced by unbalances as well as forces from the cutting process. This model can also be used to determine unbalance distributions or balancing weights, respectively, from vibration data measured at given sensors during an idle speed of the spindle.The determination of the unbalance distribution forms an ill-posed inverse problem that requires regularization techniques for its solution [4]. Secondly, we have developed an analytical process model for the description of the cutting forces during the cutting process and related those forces to the surface structure of the workpiece [5]. Since the cutting forces influence the vibrations of the machine and vice versa, both sub-models have to merge into a mechanic-dynamical model. The model will enable us to determine the effective cutting forces and displacements related to the workpiece surface. In the near future, this model will also allow us to compute the surface quality and an objective necessary balancing state to achieve a given surface quality.

2 Structural sub-model of the experimental platform

The UPCM experimental platform from Figure 2 has a complex structure which is difficult to model. We thus have to make simplifying assumptions that enable us to handle the model mathematically but also make sure that the simplified model is still a good approximation of the reality.

2.1 System matrices

First, we have divided the platform into several components which are illustrated in Figure 3. Namely, we have the rotating part of the spindle, the spindle casing, the rotating part of the engine, and the engine casing. The spindle rotor and casing are connected by an air bearing with two spherical calottes. We have modeled this bearing by two spring-damper elements although in a first attempt we have neglected any damping in the springs. The engine bearings are also modeled as spring-damper elements. Spindle and engine are connected by a coupling that can compensate deformations in axial and radial directions as well as torsion and is also modeled as a spring element. Spindle and engine are supported by a granite board that is assumed to be rigid. The joints to the granite board are modeled as firm spring elements. Figure 3 also shows the coordinate system. The spindle rotates counterclockwise around the x-axis. Secondly, we have developed a vibration model for each part of the machine separately. If we would consider unbalances as possible causes for vibrations only it would suffice to allow vibrations in radial directions y and z. Since unbalances cause harmonic vibrations, the vibrations in y and z direction are the same except for a phase shift of $\pi/2$. Nevertheless, the forces from the cutting process act in all three directions. Hence we have to describe the vibration of each point of the platform as a function $u = u(x, y, z, t)$. The vibrations u are given as solutions of a partial differential equation (PDE) or via an equivalent energy formulation. Using the Finite Element (FE) discretization in the space variables (x, y, z), this can be reduced to a system of ordinary differential equation (ODE) in time of the form

$$\mathbf{M}\ddot{\mathbf{u}}(t) + \mathbf{S}\mathbf{u}(t) = \mathbf{p}(t), \tag{1}$$

where $\mathbf{M}$ denotes the mass matrix, and $\mathbf{S}$ the stiffness matrix. In case of damping in the system we would have a third therm $\mathbf{D}\dot{\mathbf{u}}(t)$ on the left hand side with a sparse damping matrix $\mathbf{D}$. For the discretization, the considered platform parts are divided into elements with nodes at each end. The movement of each point between the nodes is described by ansatz functions scaled with the movement of the nodes. Considering the boundary and transition conditions between the end node of one element and the first node of the next element we will get system matrices $\mathbf{M}$ and $\mathbf{S}$ for each part of the platform. This procedure is well known, we have mainly followed [11] in order to derive the matrices. We have used the following partition:

1. Spindle rotor with the coupling: 36 elements.
2. Spindle casing: 30 elements.
3. Rotational part of the engine: 3 elements.
4. Engines casing: 2 elements.

Each node has 6 degrees of freedom (DOF): the displacement u, v, w in x, y, z direction, the torsion angle β_x, and the cross section slopes β_y, β_z. The DOF of each of the parts specified above are collected in vectors $\mathbf{u}_{sp-rot}, \mathbf{u}_{sp-cas}, \mathbf{u}_{e-rot}, \mathbf{u}_{e-cas}$. A discretization int N_i elements in our model leads to $N_i + 1$ nodes and thus $6 \cdot (N_i + 1)$ DOF in the model of the ith part. The vectors of DOF are subject to Equation. (1) with mass matrices $\mathbf{M}_{sp-rot}, \mathbf{M}_{sp-cas}, \mathbf{M}_{e-rot}, \mathbf{M}_{e-cas}$ and stiffness matrices $\mathbf{S}_{sp-rot}$, $\mathbf{S}_{sp-cas}$, $\mathbf{S}_{e-rot}$, $\mathbf{S}_{e-cas}$. If we collect all DOF in one vector

$$\mathbf{u} = (\mathbf{u}^T_{sp-rot}, \mathbf{u}^T_{sp-cas}, \mathbf{u}^T_{e-rot}, \mathbf{u}^T_{e-cas})^T, \tag{2}$$

we get a block diagonal structure for the entire mass matrix:

$$\mathbf{M} = \begin{pmatrix} \mathbf{M}_{sp-rot} & \mathbf{0} & \mathbf{0} & \mathbf{0} \\ \mathbf{0} & \mathbf{M}_{sp-cas} & \mathbf{0} & \mathbf{0} \\ \mathbf{0} & \mathbf{0} & \mathbf{M}_{e-rot} & \mathbf{0} \\ \mathbf{0} & \mathbf{0} & \mathbf{0} & \mathbf{M}_{e-cas} \end{pmatrix}. \tag{3}$$

The stiffness matrix $\mathbf{S}$ is arranged in the same way. So far, the matrices $\mathbf{M}$ and $\mathbf{S}$ have a block diagonal structure and the dimension 450×450. For the stiffness matrix, we have to add entries related to the bearing elements that relate the DOF of the corresponding nodes in the connected parts via a stiffness parameter C and damping parameters D. This results in off-diagonal elements for the entire stiffness matrix, and in a damping matrix $\mathbf{D}$, respectively. Stiffness values for the coupling between engine and spindle were provided by the manufacturer. For the air bearing between spindle and spindle casing we had to rely on an inspection record of the manufacturer that stated measurement values for the axial and radial stiffness of the bearing in the steady state but no information about damping properties was provided. Therefore, we have neglected the damping in a first attempt as mentioned earlier.

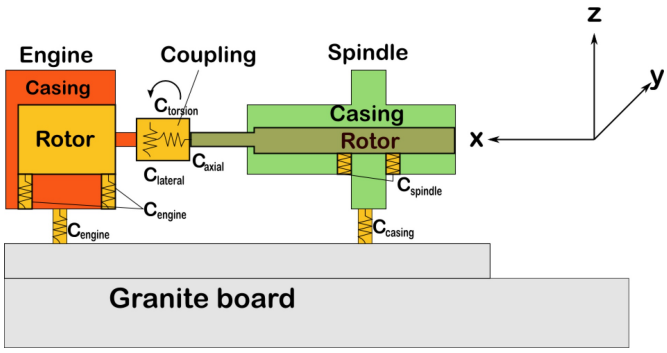

Fig. 3 Modeled parts of the platform

2.2 Model Adjustment

Although we have carefully modeled the elements with respect to their geometry and physical properties, we still made simplifications. Therefore, we can only hope, but not expect that the model fits reality immediately. The most uncertain values are the stiffness parameters for the bearings, in particular those from the air bearing. A modal analysis of the experimental platform was carried out in order to adjust the model eigenfrequencies to the eigenfrequencies of the platform but the analysis turned out to be faulty. So far, the only reliable information we have of the real platform are the vibrational data for certain defined unbalance settings in a frequency range of $[5, \cdots, 50]$ Hz. For a good model, the measured data has to fit the computed data reasonably well. With the pre-chosen model parameters we were not able to achieve this data fit immediately. Hence we have changed the stiffnesses for all bearings and monitored its effect on the vibrational response. It turned out that the stiffness of the air bearing changed the vibrational behavior most notably, i.e., a reduction of its stiffness produced a desired eigenfrequency at 15 Hz. The influence of other bearings on the lower eigenfrequencies was insignificant. A comparison of the data produced by the model with the measurements ca be seen in Figure 4. We note that, although the theoretical frequency range of the model is arbitrary, the optimization was restricted to data for the range $[5, \cdots, 50]$ Hz. This first attempt to optimize the model according to the sparse information we had was successful but it is still questionable if the model reflects the machine correctly in all necessary aspects. It is planned to carry out a new modal analysis at LFM in the near future. If these data are available, then a more reliable model can be generated. Meanwhile, we have used this model for further computations and tests, in particular the combination with the force model, but we are aware of the fact that tests with real data have to be postponed until the model is improved during the next project phase.

2.3 Solution of the vibration equation in the presence of unbalances

If we only consider unbalances in our cutting machine, the right hand side $\mathbf{p} = \mathbf{p}_{unb}(t)$ of Equation (1) has harmonic entries depending on the angular velocity ω. In practice, the revolution speed n in rpm is given, therefore we have $\omega = \frac{2\pi}{60} n$. An unbalance is modeled as a mass Δm displaced from the shaft by a vector $\mathbf{r} = re^{i \cdot \phi}$. ϕ is the angle to a given zero mark. If the displaced mass rotates with angular velocity ω it induces a centrifugal force of absolute value F :

$$F = \omega^2 b, \text{ with } b := \Delta m r.$$

The projection of this force onto the y- and z- axis yields

$$\begin{aligned} F_y &= \omega^2 b \sin(\omega t + \phi) = \Im(\omega^2 b e^{i\phi} e^{i\omega t}), \\ F_z &= \omega^2 b \cos(\omega t + \phi) = \Re(\omega^2 b e^{i\phi} e^{i\omega t}). \end{aligned}$$

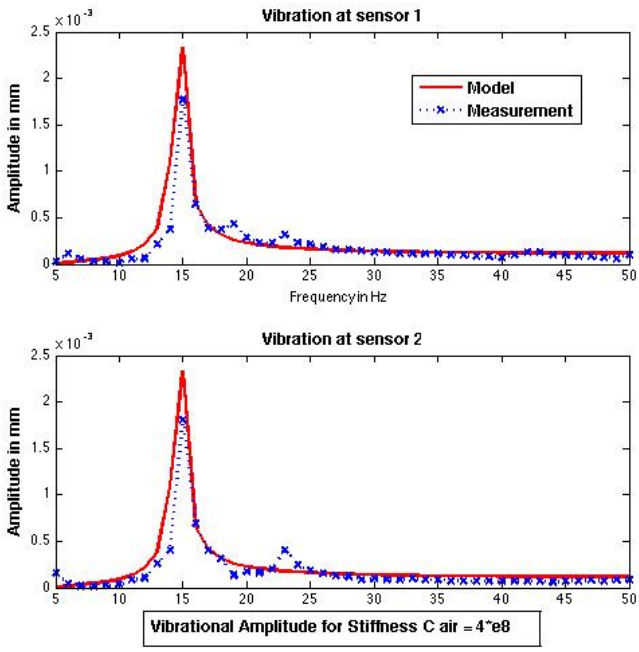

Fig. 4 Comparison of model and measurement data for given unbalance

Those forces only apply to the displacement DOF in y-direction, and z-direction, resp. All the other DOF are not affected. Therefore, the sub-vector $\mathbf{p}_k$ of $\mathbf{p}$ containing the entries for the DOF of the k-th node, $k =, \cdots, N$, has the form

$$\mathbf{p}_k = \begin{pmatrix} 0 \\ \Im(\omega^2 b_k e^{i\phi_k} e^{i\omega t}) \\ \Re(\omega^2 b_k e^{i\phi_k} e^{i\omega t}) \\ 0 \\ 0 \\ 0 \end{pmatrix}.$$

We split $\mathbf{p}_{unb}(t) = (\mathbf{p}_k)_k$ into part with $\sin$ and $\cos$ entries only in order to apply the right hand side ansatz for each of the parts to solve (1):

$$\begin{aligned} \mathbf{p}_{unb} &= \Im(\mathbf{q}^1 e^{i\omega t}) + \Re(\mathbf{q}^2 e^{i\omega t}), \text{ with } \mathbf{q}^{1,2} = (\mathbf{q}_k^{1,2})_k \\ \mathbf{q}_k^1 &= \begin{pmatrix} 0 \\ \Im(\omega^2 b_k e^{i\phi_k} e^{i\omega t}) \\ 0 \\ 0 \\ 0 \\ 0 \end{pmatrix}, \ \mathbf{q}_k^2 = \begin{pmatrix} 0 \\ 0 \\ \Re(\omega^2 b_k e^{i\phi_k} e^{i\omega t}) \\ 0 \\ 0 \\ 0 \end{pmatrix}. \end{aligned} \tag{4}$$

Inserting the equation $\mathbf{u}_{unb}^j(t) = \mathbf{u}^j e^{i\omega t}, j = 1, 2$ and its second derivative in (1) yields

$$\begin{aligned} \mathbf{u}_{unb} &= \mathbf{u}_{unb}^1(t) + \mathbf{u}_{unb}^2(t), \\ &= \Im((-\omega^2\mathbf{M} + \mathbf{S})^{-1}\mathbf{q}_1 e^{i\omega t}) + \Re((-\omega^2\mathbf{M} + \mathbf{S})^{-1}\mathbf{q}_2 e^{i\omega t}). \end{aligned} \tag{5}$$

The solution of (1) is the sum of the particular solution $\mathbf{u}_{unb}$ and the general solution of the homogeneous equation with right hand side zero. The latter will be given in Section 4. After a certain time of rotation with a constant angular velocity and no other forces than those from unbalances the homogeneous solution will die out due to small damping effects. Hence, in this case we have the solution $\mathbf{u}_{unb}$.

3 Balancing

As mentioned in the Introduction, the mounting of a workpiece onto the spindle often results in an unbalanced system. This unbalance can be projected onto the two balancing planes. Reconstructing this projected unbalance distribution allows us to determine the necessary balancing weights that have to be mounted in the balancer rings. The reconstruction is done with the help of the above given model. To this end, the workpiece has to be added to the model, i.e., we have to include an element in the rotating part of the spindle.Balancing then means to compute the balancing weights as well as their positions from measurements of the vibration.

3.1 Inverse problem

In order to determine the balancing weights from vibration measurements, we formulate the problem as an operator equation

$$\mathbf{A}(b) = u. \tag{6}$$

Here b denotes the unbalance distribution we are looking for, and u denotes the vibrations induced by this unbalance distribution measured at positions where sensors are mounted. The operator $\mathbf{A}$ has to map the unbalance distribution to the vibrational data at the sensor positions. In our case we can use (5) to describe this operator if we assume that the homogeneous solutions has already vanished. Usually this operator is not continuously invertible, which means that for given noisy data u_ε with a data error of $\varepsilon \geq \|u - u_\varepsilon\|_2$ the function $b^\varepsilon = \mathbf{A}^{-1}(u_\varepsilon)$ might be an arbitrary bad approximation of the true unbalance distribution b. Problems with those properties are referred to as being ill-posed. In this case, least square techniques, where b^ε is computed as the minimizer of $\|\mathbf{A}b - u_\varepsilon\|^2$, are unstable. The computation of b^ε can be stabilized by minimizing

$$b^\varepsilon_\alpha = \min_b [\|\mathbf{A}b - u_\varepsilon\|_2 + \alpha\Psi(b) \tag{7}$$

instead. The penalty term $\Psi(b)$ acts as a stabilizer and prevents large values of $\Psi(b)$.Typical choices of Ψ are, e.g., $\Psi(b) = \|b\|_p := \left(\sum_i |b_i|^p\right)^{1/p}$, $0 < p \leq 2$. Problems that are not continuously invertible are called ill-posed and require regularization [6]. The functional (7) is well known as Tikhonov functional and forms a regularization method [7, 8]). The parameter α is called the regularization parameter, it has to be chosen according to the amount of noise in the data and assures the convergence of b^ε_α to b as $\varepsilon \to 0$. A popular rule for the choice of α is Morozov's discrepancy principle, [9, 10].

3.2 Computations of balancing weights

In order to find the underlying unbalance distribution projected onto the balancers, we have minimized the functional (7) with $\Psi = \|.\|_2$. As the model needs a further update to perform well with real data, we have performed first tests with artificial data. We placed a specified unbalance at the node of the workpiece and used our model to compute the related vibrations of the platform. In order to simulate a real situation, we have assumed that the data can only be obtained at two sensor positions. To simulate measurements we have disturbed the data at the sensor positions with noise $(20 - 30\%)$. We have then reconstructed the unbalance projected onto the balancing planes by minimizing (7), i.e., we reconstructed an unbalance distribution that produces approximately the same vibrations at the sensors as the original unbalance created by the workpiece but is located at the two balancer positions. As an example for a unbalance created by a workpiece, we have set 50gmm at an angle of $30°$ to the zero mark at the workpiece node in the model. The corresponding amplitudes of the vibrations for a frequency range of $[5, \cdots, 50]$ Hz 'measured' at the first sensor are plotted in Figure 5 (red line without markers). The vibrations were disturbed with a noise level of 26%,.i.e. $(\|u - u^\delta\|)/\|u\| = 0.26$. In the balancing planes, we have reconstructed unbalances of 26 gmm in the first and 26.5 gmm in the second plane both with a position of $30°$. The balancing masses at the balancers can be placed on a radius $r = 41.5$ mm, thus the according masses are determined as 0.63 g in the first plane and 0.64 g in the second, both have to be placed under an angle of $210°$, see Figure 6. As is shown in Figure 5 (blue line with star markers), the setting of those balancing masses reduces the vibration amplitude significantly.

4 Sub-model for the machining process forces

The sub-model for the machining process consists of two parts: a force model to simulate the actual cutting force and a model for the actual process parameters as well as the tip of the tool position on the workpiece surface. Actual parameter means that the parameter is time dependent in contrast to the given constant input parameters at the test stand. Different turning operations are usually applied in diamond machining but we will focus on the geometrically most simplest process.

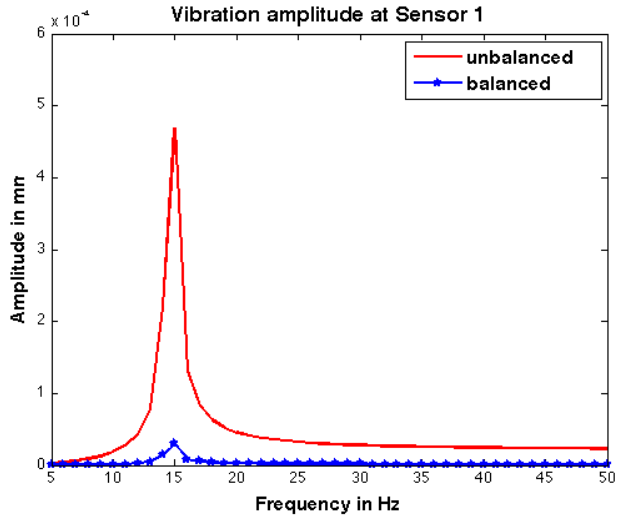

Fig. 5 Vibration amplitude for a workpiece unbalance of 50 gmm with 30° angle before and after balancing

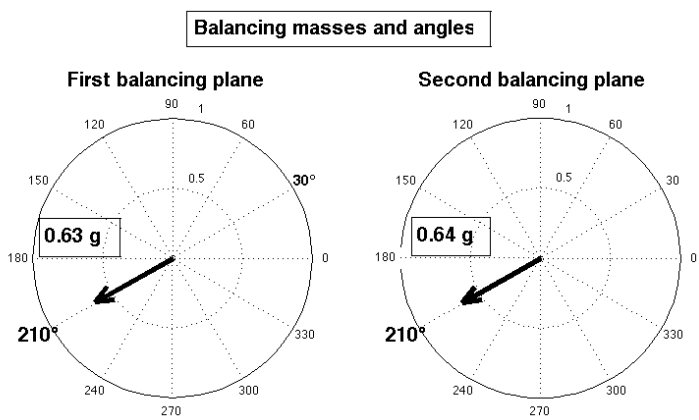

Fig. 6 Balancing masses and angles for a workpiece unbalance of 50 gmm with 30°, balancing radius = 41.5mm

Figure 7 shows a schematic diagram of the considered diamond face turning process. In face turning the tool is moving along the y-axis with a feed velocity v_f and cuts the workpiece with a depth of cut a_p at its front face. The acting force can be split in three components, the cutting force F_c in negative z-direction, the thrust force F_t in negative x-direction and the feed force F_f in negative y-direction. In the considered process, the cutting velocity

$$v_c(t) = 2\pi n(r - d(t)) \tag{8}$$

is decreasing with time since the rotational speed n is constant but the traveled distance d is increasing (see Figure 7). Therefore, we need a force model that includes the cutting velocity v_c in addition to the depth of cut, a_p, and the feed rate f. The feed rate f is defined as the distance the diamond tool is traveling during one revolution.

4.1 Force model

For conventional cutting processes there are well-established standard force models (e.g. [12]), whereas the development of force models for micro-cutting is an actual topic of research, because so called size effects like, e.g., ploughing, the cutting edge radius and minimum uncut chip thickness have to be taken into account. For an overview about size effects

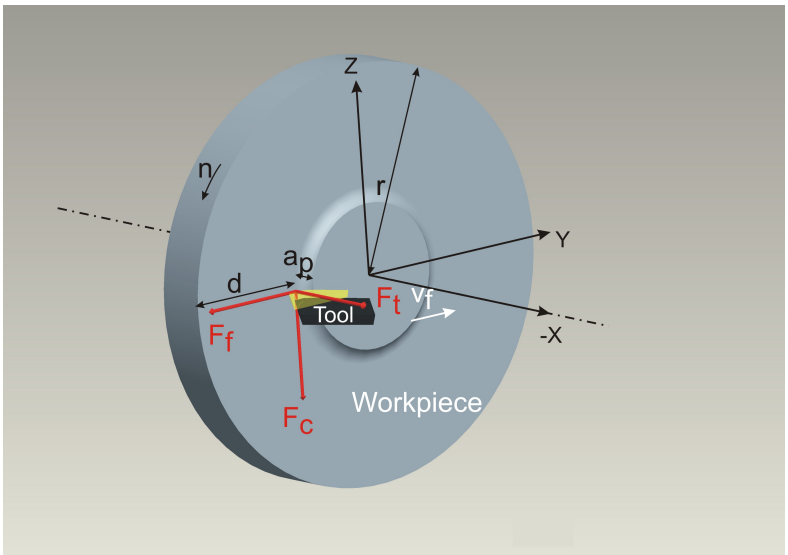

Fig. 7 Schematic diagram of the face turning process and the tree force components of the acting force: cutting force F_c, thrust force F_t and feed force F_f.

in manufacturing we refer to [13]. In ultra-precision turning the situation is exceptional. Due to the use of diamond tools, cutting parameters like depth of cut and feed rate are in the range of some micrometers. Diamond tools lead to sharper cutting edges than conventional (carbide) tools. Therefore, some size effects like ploughing play only a subordinate role in diamond machining. Nevertheless the forces in our experiment show a typical behavior for micro machining with the used workpiece material (aluminum alloy: AlMg3). I.e. the thrust force is the dominant force component and the forces are in the range of one Newton or less because of the small depth of cut. Because of this special characteristics and the fact that most of the force models do not include varying cutting velocities we built up our own force model which we calibrated with force measurements.

The starting point for the force model is the Kinzle model, see for example [14], i.e. the cutting force components $F_i,\ (i = t, f, c)$, are proportional to the cross section area of cut A_c and can be computed using the specific cutting force components k_t, k_f, k_c

$$F_i = k_i A_c \quad (i = c, t, f). \tag{9}$$

The cross sectional area of cut A_c can be approximated by the product of depth of cut a_p and feed rate f, i.e. $A_c = a_p f$. In the next subsection we present a method to calculate time dependent process parameters $a_p(t)$ and $f(t)$ in order to calculate the actual forces. To model the specific force components a recently proposed modified Kienzle model [15] is used as starting point. The basic idea of this model is a product ansatz for the specific force, e.g. the specific k_c

$$k_c = f_1(a_p) f_2(v_c) f_3(r_\beta) f_4(\mu), \tag{10}$$

where r_β denotes the cutting edge radius and μ the friction coefficient. In our experiments f_3 and f_4 are constant, but the cutting depth a_p and the cutting velocity v_c vary. From [15] we applied the formula for f_1 and f_2

$$k_c(t) = \left(\alpha_1 v_c(t)^{\beta_1} + \alpha_2 v_c(t)^{-\beta_2}\right)\left(C\, a_p(t)^{-m_c}\right) \tag{11}$$

with model constants C, m_c, α_i, β_i $(i = 1, 2)$. The constant functions f_3 and f_4 are included in C. A similar ansatz can be made for the specific thrust force k_t and specific feed force k_f. In order to determine the model constants we have used force measurements which had been performed by the LFM. The parameter in those measurements were the feed velocity $v_f = 8\,mm/min$, and the rotational speed $n = 1500\,rev/min$. The depth of cut a_p has been varied between 2 and $14\mu m$. The workpiece radius r is $30\,mm$. We have optimized the model parameters C, m_c, α_i, β_i $(i = 1, 2)$ in order to fit the measurement data for the forces. As this worked well, this is also a confirmation that our model assumptions were correct in the sense that the model approximates the reality very well. Figure 8 shows on the left hand side the specific force measurements over depth of cut and the fitted curve $f_1(a_p)$ as red solid line. On the right side the experimental measurements and the model simulation using the equation (11) of the cutting and thrust force for a depth of cut of $5\mu m$ are shown.

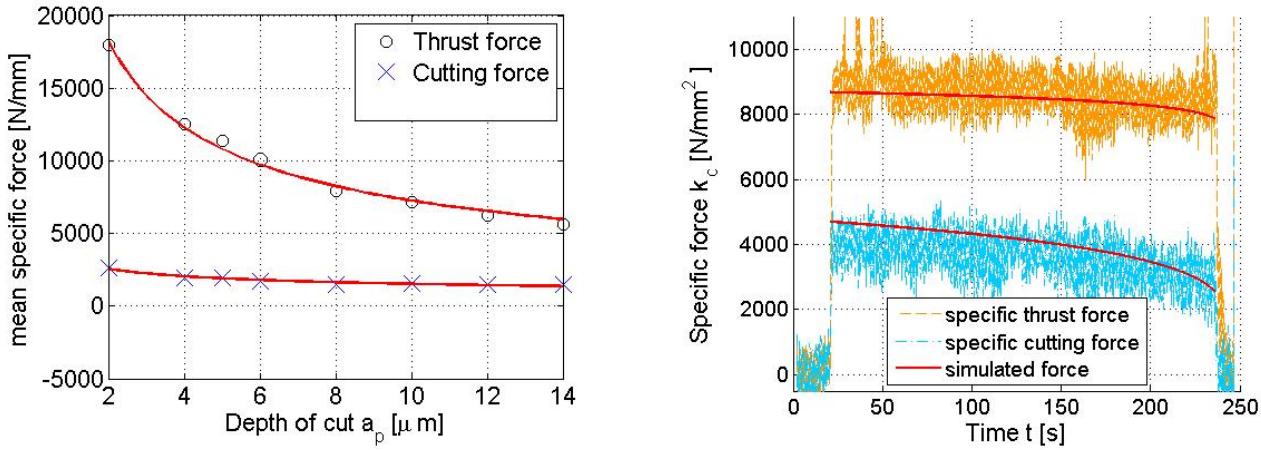

Fig. 8 Comparison between force measurement and simulation: Mean specific force over depth of cut (left) and specific forces over time (and hence over cutting velocity) for a depth of cut of $a_p = 5\mu m$ (right).

4.2 Simulation of the tool path on the workpiece surface

The second part of the process sub-model is a model for the actual process parameters and the actual tool path which is the basis for simulating the machined surface. Here we have followed a method proposed in [5]. The actual position of the tool is given by

$$x(t) = a_p - \frac{1}{2l_h}\left(\delta_x^2 + \delta_y^2\right) - \delta_x - \Delta_x(t) + (r - d(t))\tan\left(\beta_y(t)\right)\,, \tag{12}$$

$$y(t) = -r + v_f t \qquad -\delta_y - \Delta_y(t)\,, \tag{13}$$

$$z(t) = \qquad -\delta_z - \Delta_z(t)\,, \tag{14}$$

where Δ_i are the displacements of the workpiece induced by vibrations caused by unbalances, and δ_i, $i \in \{x, y, z\}$, are the deflections of the tool holder of length l_h. The angle β_y denotes the rotation of the workpiece around the z-axis. This tilt of the workpiece can influence the actual depth of the cut a_p which is described in Equation (12). The feed velocity can be determined by the feed rate f as $v_f = nf$. The deflections of the workpiece and the tool reduce the cutting depth a_p, see equation (12), and change the real feed velocity v_f. Therefore, we now assume a time dependence of the actual process parameter, namely the actual depth of cut

$$a_p(t) = x(t) \tag{15}$$

and the actual feed velocity

$$v_f(t) = \dot{d}(t)\,, \text{ with } d(t) = y(t) - r. \tag{16}$$

Hence the actual feed rate is

$$f(t) = n^{-1} v_f(t). \tag{17}$$

These actual process parameters are plugged into the formulae (8) and (9) for the force components using the equations for the specific forces. Using the actual forces, we are now able to determine the deflections of the tool holder which are proportional to the forces

$$\delta_x(t) = \frac{F_t(t)}{k_{ex}}\,,\ \delta_y(t) = \frac{F_f(t)}{k_{ey}}\,,\ \delta_z(t) = \frac{F_c(t)}{k_{ez}}\,. \tag{18}$$

Here k_{ei} denotes the corresponding stiffness in the directions $i \in \{x, y, z\}$, (not to mix up with the specific forces k_t, k_f, k_c). Since all force components have the same structure we get for all three spatial directions

$$\delta_i(t) = k_{ei}^{-1}\left(\alpha_1^i v_c(t)^{\beta_1^i} + \alpha_2^i v_c(t)^{-\beta_2^i}\right)\left(C_i\, a_p(t)^{-m_i}\right) a_p(t) f(t) \tag{19}$$

for the deflection in direction $i \in \{x, y, z\}$. Further, derivatives of the equations (12)-(14) for the actual position and the deflections (19) combined with the formulae (15) and (16) give a system of differential equations as follows:

$$\dot{\delta}_x(t) = \frac{1}{nk_{ex}} \left(\dot{k}_t(t) a_p(t) v_y(t) + k_t(t) \left[\dot{a}_p(t) v_y(t) + a_p(t) \dot{v}_y(t) \right] \right) , \tag{20}$$

$$\dot{\delta}_y(t) = v_f - v_y(t) - \dot{\Delta}_y(t) , \tag{21}$$

$$\dot{\delta}_z(t) = \frac{1}{nk_{ez}} \left(\dot{k}_c(t) a_p(t) v_y(t) + k_c(t) \left[\dot{a}_p(t) v_y(t) + a_p(t) \dot{v}_y(t) \right] \right) , \tag{22}$$

$$\dot{v}_y(t) = \frac{\dot{\delta}_y(t) - n^{-1} k_{ey}^{-1} v_y(t) \left(\dot{k}_f(t) a_p(t) - k_f(t) \dot{a}_p(t) \right)}{n^{-1} k_{ey}^{-1} k_f(t) a_p(t)} , \tag{23}$$

$$\dot{a}_p(t) = -\frac{1}{l_h} \left(\delta_y(t) \dot{\delta}_y(t) + \delta_z(t) \dot{\delta}_z(t) \right) - \dot{\delta}_x(t) - \dot{\Delta}_x(t) , \tag{24}$$

$$+ (r - d_y(t)) \frac{\dot{\beta}_y(t)}{\cos^2(\beta_y(t))} - v_y(t) \tan(\beta_y(t)) , \tag{25}$$

$$\dot{d}(t) = v_y(t) , \tag{26}$$

$$\begin{aligned} \dot{k}_t(t) = & -m_x C_x a_p(t)^{-m_x - 1} \dot{a}_p(t) \left(\alpha_1^x v_c(t)^{\beta_1^x} + \alpha_2^x v_c(t)^{-\beta_2^x} \right) \\ & - C_x a_p(t)^{-m_x} v_y(t) \left(\alpha_1^x \beta_1^x v_c(t)^{\beta_1^x - 1} - \alpha_2^x \beta_2^x v_c(t)^{-\beta_2^x - 1} \right) , \end{aligned} \tag{27}$$

$$\begin{aligned} \dot{k}_f(t) = & -m_y C_y a_p(t)^{-m_y - 1} \dot{a}_p(t) \left(\alpha_1^y v_c(t)^{\beta_1^y} + \alpha_2^y v_c(t)^{-\beta_2^y} \right) \\ & - C_y a_p(t)^{-m_y} v_y(t) \left(\alpha_1^y \beta_1^y v_c(t)^{\beta_1^y - 1} - \alpha_2^y \beta_2^y v_c(t)^{-\beta_2^y - 1} \right) , \end{aligned} \tag{28}$$

$$\begin{aligned} \dot{k}_c(t) = & -m_z C_z a_p(t)^{-m_z - 1} \dot{a}_p(t) \left(\alpha_1^z v_c(t)^{\beta_1^z} + \alpha_2^z v_c(t)^{-\beta_2^z} \right) \\ & - C_z a_p(t)^{-m_z} v_y(t) \left(\alpha_1^z \beta_1^z v_c(t)^{\beta_1^z - 1} - \alpha_2^z \beta_2^z v_c(t)^{-\beta_2^z - 1} \right) . \end{aligned} \tag{29}$$

The cutting velocity is calculated by $v_c(t) = 2\pi n (r - d(t))$ and the vibrations Δ_i, $i \in \{x, y, z\}$, as well as the tilt angle β_y of the workpiece and their derivatives are determined by the structural sub-model. The system of differential equations will be solved numerically with the MATLAB solver ode15i. The stiffness values k_{ei} $(i = x, y, z)$ are determined by the geometrical dimensions of the tool holder and its elasticity module (material: steel, $E = 210kN/mm^2$). The resulting actual forces F are calculated by the deflections δ using equation (18). The numerical results are presented in Section 5.

5 Coupling of the sub-models

In the last two Sections we have developed two sub-models, one describing the displacement or vibration behavior of the cutting machine in the nodes of an FE model via the solution of (1), and one that computes the forces (F_t, F_f, F_c) and the deflections of the tool holder $(\delta_x, \delta_y, \delta_z)$ during the cutting process. So far, they are separated, but in practice they influence each other: the forces from the cutting process add to the forces from unbalances in the right hand side of Equation (1) in the vibration model, whereas the resulting displacements in the first node (workpiece) of the vibration model influence the cutting forces and the actual deflection of the tool. The additional load vector from the cutting forces and moments in the right hand side of Equation (1) has the form

$$\mathbf{p}_{cut}(t, \mathbf{u}(t)) = (F_t, F_f, F_c, M_t, 0, M_c, 0, \cdots, 0)^T, \text{ with } M_{\{t,c\}} = F_{\{t,c\}} \times r_a, \tag{30}$$

where $r_a(t) = r - d(t)$ denotes the radius of the workpiece minus the already traveled distance of the tool on the workpiece, cf. Figure 7. The dependence of $\mathbf{p}_{cut}$ on $\mathbf{u}$ is that the deflections of the tool equals the first three entries of $\mathbf{u}$:

$$(\Delta_x, \Delta_y, \Delta_z) = (u_1, u_2, u_3). \tag{31}$$

Thus, the right hand side of Equation (1) depends also on its solution, i.e., we have to deal with a nonlinear problem that cannot be solved explicitly. In order to solve the system approximately, we have employed a time step algorithm and assumed the forces and moments from the cutting process to be constant during a small time interval, i.e. $\mathbf{p}_{cut}(t) = \mathbf{p}_{cut}(t_i)$ for $t \in [t_i, t_i + \Delta t]$. Now,

$$\mathbf{u}(t) = A(\mathbf{p}_{unb} + \mathbf{p}_{cut}(t_i)), \; t \in [t_i, t_i + \Delta t],$$

where A describes the solution operator of (1). The resulting deflections $(\delta_x, \delta_y, \delta_z)$ from (31) are plugged into the force model and we compute

$$(F_t(t_{i+1}), F_f(t_{i+1}), F_c(t_{i+1})) = B(\mathbf{u}(t_i + \Delta t)) = B(\delta_x, \delta_y, \delta_z)$$

at $t_{i+1} = t_i + \Delta t$. Here B denotes the solution operator for solving (20)-(29) and use (18) afterwards. Again, we assume the cutting forces to be constant over the next time interval $[t_{i+1}, t_{i+1} + \Delta t]$. We repeat this routine untill we reach the end of the desired time interval $t \in [t_0, t_{end}]$, for which we want to solve our combined system.

5.1 Solution of the differential equation

Since our problem is linear, the solution of the vibration equation (1) in the presence of unbalances and cutting forces is the sum of the general solution of the homogeneous equation $\mathbf{u}_h(t)$ and particular solutions $\mathbf{u}_{unb}(t)$ and $\mathbf{u}_{cut}(t)$ for the right hand sides $\mathbf{p}_{unb}$ and $\mathbf{p}_{cut}$. The initial conditions for Equation (1) on the interval $(t_j, t_{j+1}]$, are given by

$$\mathbf{u}(t_j) = \mathbf{u}_h(t_j) + \mathbf{u}_{imb}(t_j) + \mathbf{u}_{cut}(t_j), \tag{32}$$

$$\dot{\mathbf{u}}(t_j) = \dot{\mathbf{u}}_h(t_j) + \dot{\mathbf{u}}_{imb}(t_j) + \dot{\mathbf{u}}_{cut}(t_j). \tag{33}$$

The solution $\mathbf{u}_{unb}(t)$ was already presented in Section 2.3. To compute $\mathbf{u}_h$ and $\mathbf{u}_{cut}$, we multiply (1) from the left with $\mathbf{M}^{-1}$ and compute the Eigenvalue decomposition of $\mathbf{M}^{-1}\mathbf{S}$, which can be done with MATLAB, i.e., we have

$$\mathbf{M}^{-1}\mathbf{S} = \mathbf{V}\mathbf{\Phi}\mathbf{V}^{-1},$$

where $\mathbf{\Phi}$ is a diagonal matrix of Eigenvalues λ_i and $\mathbf{V}$ is the matrix containing the corresponding Eigenvectors as columns. Inserting the decomposition into (1), multiplying again from the left with $\mathbf{V}^{-1}$ we arrive at

$$\mathbf{V}^{-1}\ddot{\mathbf{u}} + \mathbf{\Phi}\mathbf{V}^{-1}\mathbf{u} = \mathbf{V}^{-1}\mathbf{M}^{-1}\mathbf{p}_{cut}.$$

Defining

$$\mathbf{q} := \mathbf{V}^{-1}\mathbf{u},\ \mathbf{c} := \mathbf{V}^{-1}\mathbf{M}^{-1}\mathbf{p}_{cut}$$

we get a decoupled system

$$\ddot{\mathbf{q}} + \mathbf{\Phi}\mathbf{q} = \mathbf{c}.$$

In this form we can easily find the solution of the homogeneous equation and the equation with constant right hand side $\mathbf{c}$. For $\mathbf{u}_{cut}$ we get

$$q_j(t) = \frac{c_j}{\lambda_j}(1 - \cos(\sqrt{\lambda_j} \cdot t)),\ 1 \le j \le n, \text{ or}$$

$$\mathbf{u}_{cut}(t) = \mathbf{V}\mathbf{q}(t) = \mathbf{V}[\mathbf{I} - \cos(\mathbf{\Phi}^{1/2}t)]\mathbf{\Phi}^{-1}\mathbf{c}, \text{ and} \tag{34}$$

$$\dot{\mathbf{u}}_{cut}(t) = \mathbf{V}\sin(\mathbf{\Phi}^{1/2}t)\mathbf{\Phi}^{-1/2}\mathbf{c}. \tag{35}$$

Here we have defined

$$\cos(\mathbf{\Phi}^{1/2}t) := \begin{pmatrix} \cos\sqrt{\lambda_1}t & \cdots & 0 \\ \vdots & \ddots & \vdots \\ 0 & \cdots & \cos\sqrt{\lambda_N}t \end{pmatrix}, \mathbf{\Phi}^{-1} := \begin{pmatrix} 1/\lambda_1 & \cdots & 0 \\ \vdots & \ddots & \vdots \\ 0 & \cdots & 1/\lambda_N \end{pmatrix}.$$

$\sin(\mathbf{\Phi}^{1/2}t)$ is defined analogously. $\mathbf{u}_h$ is the real part of the complex solution

$$\mathbf{u}_h^c(t) = \mathbf{V}\left[\exp(i\sqrt{\mathbf{\Phi}}t)\mathbf{A}^+ + \exp(-i\sqrt{\mathbf{\Phi}}t)\mathbf{A}^-\right],$$

with

$$\mathbf{A}^\pm = \begin{pmatrix} A_1^\pm \\ \vdots \\ A_N^\pm \end{pmatrix},\ \exp(\pm i\sqrt{\mathbf{\Phi}}t) := \begin{pmatrix} \exp(\pm i\sqrt{\lambda_1}t) & \cdots & 0 \\ \vdots & \ddots & \vdots \\ 0 & \cdots & \exp(\pm i\sqrt{\lambda_N}t) \end{pmatrix}.$$

The coefficients $\mathbf{A}^\pm$ have to be computed using the initial values $\mathbf{u}_h^c(t_0)$ and the derivative of $\dot{\mathbf{u}}_h^c(t_0)$:

$$\dot{\mathbf{u}}_h^c(t_0) = \mathbf{V}\left[i\exp(i\sqrt{\mathbf{\Phi}}t_0)\sqrt{\mathbf{\Phi}}\mathbf{A}^+ - i\exp(-i\sqrt{\mathbf{\Phi}}t_0)\sqrt{\mathbf{\Phi}}\mathbf{A}^-\right].$$

Hence we have to solve the system

$$\begin{pmatrix} \mathbf{u}_h^c(t_0) \\ \dot{\mathbf{u}}_h^c(t_0) \end{pmatrix} = \begin{pmatrix} \mathbf{V}\exp(i\sqrt{\mathbf{\Phi}}t_0) & \mathbf{V}\exp(-i\sqrt{\mathbf{\Phi}}t_0) \\ i\mathbf{V}\exp(i\sqrt{\mathbf{\Phi}}t_0)\sqrt{\mathbf{\Phi}} & -i\mathbf{V}\exp(-i\sqrt{\mathbf{\Phi}}t_0)\sqrt{\mathbf{\Phi}} \end{pmatrix} \begin{pmatrix} \mathbf{A}^+ \\ \mathbf{A}^- \end{pmatrix} \tag{36}$$

for $\mathbf{A}^+$ and $\mathbf{A}^-$.

5.2 Algorithm

As explained above, we have coupled the systems via a time step algorithm. We assume that at the beginning $t = t_0$ the machine is rotating with a constant rotational speed ω. As the cutting process has not yet started, the cutting forces are zero. Further we assume an unbalance distribution in the spindle that results in a load $\mathbf{p}_{unb}$. We also assume that the homogeneous solution in this case has already died out. Hence, the solution for $t = t_0$ is given by (4) and its derivative can be easily computed.

Initial solution at $\mathbf{t = t_0}$:

$$\begin{aligned} \mathbf{u}(t_0) &= \mathbf{u}_{unb}(t_0) = \Im((-\omega^2\mathbf{M}+\mathbf{S})^{-1}\mathbf{q}_1\exp(i\omega t_0)) + \Re((-\omega^2\mathbf{M}+\mathbf{S})^{-1}\mathbf{q}_2\exp(i\omega t_0)), \\ \dot{\mathbf{u}}(t_0) &= \dot{\mathbf{u}}_{unb}(t_0) = \Im(i\omega(-\omega^2\mathbf{M}+\mathbf{S})^{-1}\mathbf{q}_1\exp(i\omega t_0)) + \Re(i\omega(-\omega^2\mathbf{M}+\mathbf{S})^{-1}\mathbf{q}_2\exp(i\omega t_0)). \end{aligned}$$

$\mathbf{t} \in (\mathbf{t_0}, \mathbf{t_1}]$:
Now the cutting process starts. The computation of $\mathbf{p}_{cut}(t_0, \mathbf{u}(t_0))$ via (20)-(29) and (18) takes into account the displacement of the workpiece at time t_0 induced by the unbalance. We assume in the (short) time interval a constant cutting force $\mathbf{p}_{cut}(t) = \mathbf{p}_{cut}(t_0)$. The corresponding solution $\mathbf{u}_{cut}(t)$ of (1) for this constant cutting force is given by (see (34))

$$\mathbf{u}_{cut}(t) = \mathbf{V}[\mathbf{I} - \cos(\mathbf{\Phi}^{1/2}t)]\mathbf{\Phi}^{-1}\mathbf{V}^{-1}\mathbf{M}^{-1}\mathbf{p}_{cut},\ t \in (t_0, t_1].$$

The unbalance related solution is the same as in the initial step except with t instead of t_0. The complex solution of the homogeneous equation and its derivative are given by (36). The initial values for this differential equation are

$$\begin{aligned} \mathbf{u}(t_0) &= \mathbf{V}\left[\exp(i\mathbf{\Phi}^{1/2}t_0)\mathbf{A}^+ + \exp(-i\mathbf{\Phi}^{1/2}t_0)\mathbf{A}^-\right] + \mathbf{u}_{cut}(t_0) + \mathbf{u}_{unb}(t_0), \\ \dot{\mathbf{u}}(t_0) &= \mathbf{V}\left[ie^{i\mathbf{\Phi}^{1/2}t_0}\mathbf{\Phi}^{1/2}\mathbf{A}^+ - ie^{-i\mathbf{\Phi}^{1/2}t_0}\mathbf{\Phi}^{1/2}\mathbf{A}^-\right] + \dot{\mathbf{u}}_{cut}(t_0) + \dot{\mathbf{u}}_{unb}(t_0). \end{aligned}$$

Therefore we compute

$$\begin{pmatrix} \mathbf{A}^+ \\ \mathbf{A}^- \end{pmatrix} = \begin{pmatrix} \mathbf{V}e^{i\sqrt{\mathbf{\Phi}}t_0} & \mathbf{V}e^{-i\sqrt{\mathbf{\Phi}}t_0} \\ i\mathbf{V}e^{i\sqrt{\mathbf{\Phi}}t_0}\sqrt{\mathbf{\Phi}} & -i\mathbf{V}e^{-i\sqrt{\mathbf{\Phi}}t_0}\sqrt{\mathbf{\Phi}} \end{pmatrix}^{-1} \begin{pmatrix} \mathbf{u}(t_0) - \mathbf{u}_{cut}(t_0) - \mathbf{u}_{imb}(t_0) \\ \dot{\mathbf{u}}(t_0) - \dot{\mathbf{u}}_{cut}(t_0) - \dot{\mathbf{u}}_{imb}(t_0) \end{pmatrix}.$$

and can now give $\mathbf{u}_h(t)$ as the real part of $\mathbf{u}_h^c(t)$ in (36) with the computed coefficients $\mathbf{A}^+$ and $\mathbf{A}^-$, and we have

$$\mathbf{u}(t) = \mathbf{u}_h(t) + \mathbf{u}_{cut}(t) + \mathbf{u}_{imb}(t),\ t \in (t_0, t_1] \tag{37}$$

$$\dot{\mathbf{u}}(t) = \dot{\mathbf{u}}_h(t) + \dot{\mathbf{u}}_{cut}(t) + \dot{\mathbf{u}}_{imb}(t). \tag{38}$$

This gives us the initial values $t \in (t_1, t_2]$ and allow the computation of the cutting force $\mathbf{p}_{cut}(t_1, \mathbf{u}(t_1))$ for the next time step. This procedure is repeated for each time step. We have tested the algorithm with different time steps. The experiments showed that, especially for larger frequencies, the time resolution Δt should be smaller or equal 10^{-3}.

5.3 Numerical simulations

We have tested the algorithm for several parameter settings. As expected, the presence of unbalances mainly affects the deflection or vibration amplitudes in radial direction y and z. Nevertheless, the deflection in x direction is affected, too. We can also observe quantitative effects for unbalance distributions of different magnitude. Here, we will only present one example with the following parameters: initial depth of cut $a_p = 5\mu m$, feed rate $f = 5.33\mu m/rev$, rotational speed $n = 25$ Hz, radius of the workpiece $r = 30$ mm, tool holder length $l_h = 25$mm, time step $\Delta t = 0.001$s. We have used two different set of unbalance distributions $\mathbf{f}_1 = ([22.4gmm, 63°], [4.5gmm, 243°], [4.7gmm, 2°])$ and $\mathbf{f}_2 = ([22.4, 63°], [0.45, 243°], [0.47, 2°])$, the first position is the workpiece, the second and the third are the balancer planes.

In Figure 9 we have shown the development of the deflection over time for both unbalance settings. The vibration in y-direction as well as the development of the depth of cut are shown in Figure 10. Figure 11 presents the thrust force F_t that acts in the negative x-direction, and the cutting force F_c that acts in negative z-direction.

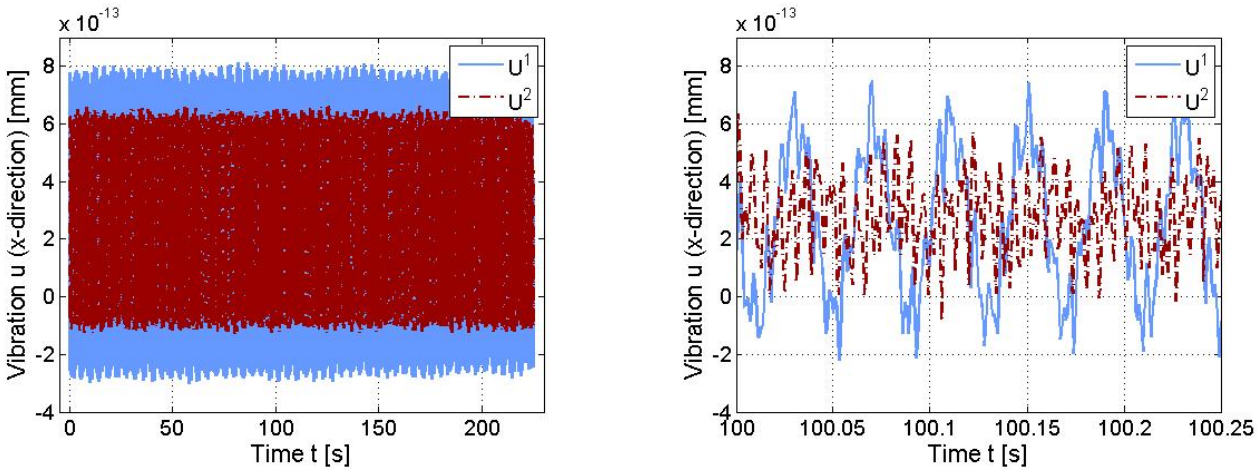

Fig. 9 Deflection in x-direction for $\mathbf{f}_1$ and $\mathbf{f}_2$; entire time interval (left), and detail (right)

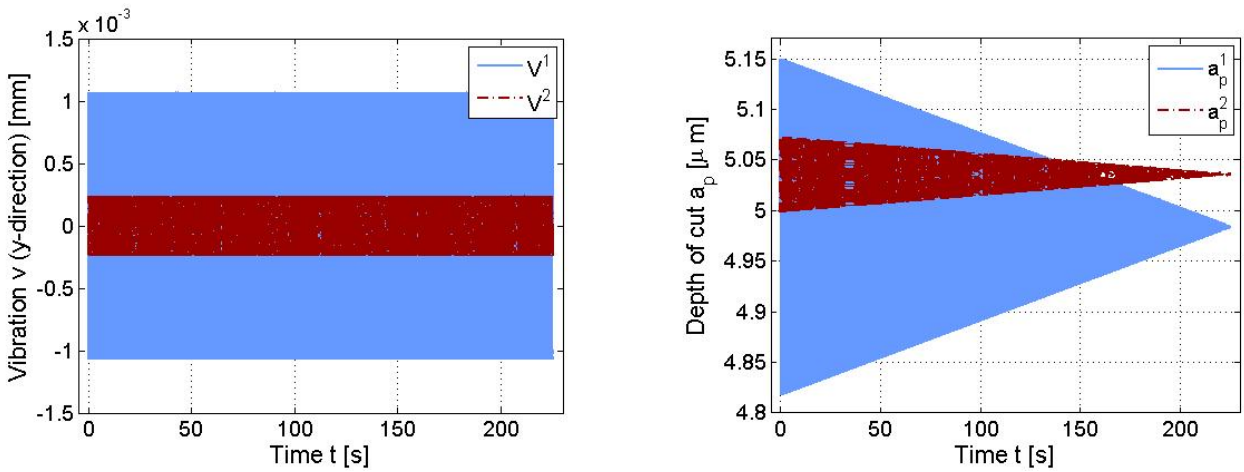

Fig. 10 Deflection in y-direction for $\mathbf{f}_1$ and $\mathbf{f}_2$; cutting depth

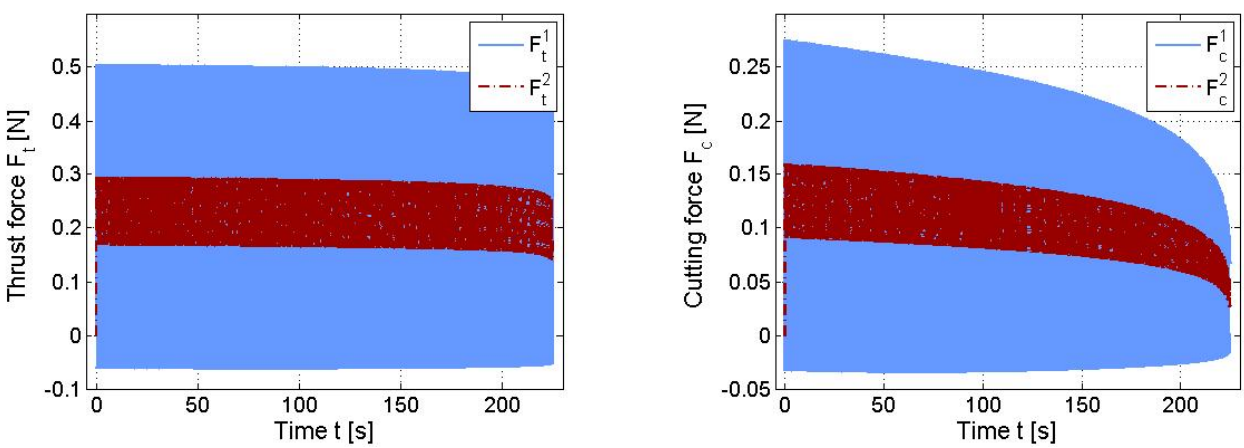

Fig. 11 Thrust force (left) and cutting force (right) for $\mathbf{f}_1$ and $\mathbf{f}_2$

6 Summary and prospect

The aim of this paper is the description of the relation of the balancing state and the surface quality in ultra-precision cutting machinery. The mathematical modeling of this connection will enable us to predict the surface quality of a workpiece for a given balancing state of the machine as well as to compute an objective necessary balancing state for a given surface quality. Additionally, the necessary balancing weights can be determined efficiently from vibrational measurements at the casing of the machine. This will lead to immense time reduction in the process of preparing the machine for the cutting process with a desired accuracy. In this paper, the goal was achieved for an experimental platform. First, a structural model was developed that can be used to determine the vibrations of the machine for given force and moment distributions, arising from unbalances and from the cutting process itself. Secondly, a model for the cutting forces and deflections was derived. It computes the actual value of those terms depending on the process parameters and the workpiece vibrations. Both models interact in a nonlinear way, i.e., using a time step algorithm, we are able to determine the relative position of the workpiece and the tool. This is the basis for the determination of the surface and the surface quality using a surface modeling program that is under development. The surface modeling and the related surface quality will be presented in a future paper.

Acknowledgements The author would like to thank Dipl.-Ing. Andreas Krause and Dr.-Ing. Oltmann Riemer from the Laboratory of Precision Machining (LFM) in Bremen, Germany, for the fruitful cooperation and the allocation of data.
The work was supported by the grant MA 1657/17-2 from the Deutsche Forschungsgemeinschaft (DFG) and grant 20237-N14 from the Austrian Science Foundation (FWF).

References

[1] E. Brinksmeier, O. Riemer: Deterministic Production of Complex Optical Elements. *Int. Jour. of Production Engineering and Computers- Special Issue on CAPP and Advances in Cutting Technology* **4 (5)**, 2002, pp. 63-72.
[2] S. Zhou, J. Shi: Active Balancing and Vibration Control of Rotating Machinery: A Survey. *The Shock and Vibration Digest* **33 (5)**, 2001, pp. 361-371.
[3] C. Brandt, H. R. Karimi, I. Piotrowska, J. Niebsch, R. Ramlau, A. Krause, O. Riemer, P. Maass: Process- Machine Interaction Model for Turning Process. *Proceedings of the 1st International Conference on Process Machine Interactions*, Hannover, 2008, pp. 239-246
[4] Niebsch, J., and Ramlau, R., Imbalances in High Precision Cutting Machinery. *Proceedings of the ASME 2009 IDETC/CIE*. San Diego, 2009,DETC/VIB-86937 .
[5] Piotkowska, I., Brandt, Ch., Karimi, H. R., Maass, P., Mathematical model of micro turning process. *The International Journal of Advanced Manufacturing Technology*, **45**, 2009, pp. 33-40.
[6] Engl, H. W., Hanke, M. and Neubauer, A., *Regularization of Inverse Problems*. Kluwer, Dordrecht, 1996.
[7] Ramlau, R., "A steepest descent algorithm for the global minimization of the Tikhonov– functional", *Inverse Problems* **18**(2), pp. 381-405, 2002.
[8] Ramlau, R., "TIGRA–an iterative algorithm for regularizing nonlinear ill–posed problem", *Inverse Problems* **19**(2), pp. 433-467, 2003.
[9] Scherzer, O., "The use of Morozov's discrepancy principle for Tikhonov regularization for solving nonlinear ill–posed problems", *Computing*, **51**, pp. 45-60, 1993.
[10] Ramlau, R., "Morozov's Discrepancy Principle for Tikhonov regularization of nonlinear operators", *Numer. Funct. Anal. and Optimization*, **23**(1&2), pp. 147–172, 2002.
[11] Gasch, R. and Knothe, K., *Strukturdynamik 2*. Springer, Berlin, 1989.
[12] Altintas, Yusuf.: Manufacturing Automation: Metal Cutting Mechanics, Machine Tool Vibrations, and CNC Design, *Cambridge Univ. Press*, 2000.
[13] F. Vollertsen and D. Biermann and H.N. Hansen and I.S. Jawahir and K. Kuzman: "Size effects in manufacturing of metallic components", *CIRP Annals - Manufacturing Technology*, **58**(2), pp. 566 - 587, 2009.
[14] Tönshoff, Hans Kurt and Denkena, Berend.: Spanen: Grundlagen, *Springer Berlin etc.*, 2004.
[15] Weber, M., Autenrieth, H., Kotschenreuther, J., Gumbsch, P., Schulze, V., Lohe, D. and Fleischer, J., "Influence of friction and process parameters on the specific cutting force and surface characteristics in micro cutting", *Machining Science and Technology*, **12 (24)**, pp. 474-497, 2008.